Journal of Natural Sciences and Mathematics Research
J. Nat. Scien. & Math. Res. Vol. 11 No. 2 (2025) 122-135
ISSN: 2460-4453 (Online); 2614-6487 (Printed)
Available online at http://journal.walisongo.ac.id/index.php/jnsmr

Mineralogical classification and impact simulation of the Punggur (H7-Melt Breccia) Meteorite, Indonesia

Robiatul Muztaba[1]*, Danni Gathot Harbowo[2], Achmad Zainur Rozzykin[1], Hakim Luthfi Malasan[3]
[1]Department of Atmospheric and Planetary Science, Institut Teknologi Sumatera, Lampung, 35365, Indonesia
[2]Departement of Geology Enginering, Institut Teknologi Sumatera, Lampung, 35365, Indonesia
[3]Department of Astronomy, Institut Teknologi Bandung, Bandung, 40132, Indonesia

* Corresponding author's e-mail: robiatul.muztaba@sap.itera.ac.id

ABSTRACT

Meteorite falls in Indonesia are rarely examined through systematic scientific analysis, resulting in limited documentation of fall events and incomplete classification of recovered specimens. The Punggur meteorite fall of 28 January 2021 reportedly produced at least five fragments. This study addresses that gap by analyzing two fragments (PM-01 and PM-02) to confirm their extraterrestrial origin and to characterize their physical, chemical, and mineralogical properties. Physical characterization involved measurements of density, magnetic susceptibility, and surface morphology. The chemical composition was determined using X-ray fluorescence (XRF), while microscopic imaging was employed to compare fusion-crust features with interior textures. A web-based meteoroid-impact modeling tool was further employed to estimate the atmospheric entry behavior and environmental effects of the fall. The result is that PM-01 has dimensions of 13 × 6.5 × 8 cm, a volume of 419 mL, a mass of 2200 g, and a density of 5.25 ± 0.26 g/cm^3. PM-02 measures 25 × 23 × 16 cm, with a volume of 443 mL, a mass of 1820 g, and a density of 4.06 ± 0.06 g cm^{-3}. Modeling results indicate that post-airburst fragments retained a residual velocity of approximately 16.2 km s^{-1}, while the airburst released an estimated 2.12 × 10^{10} J of energy (0.51 × 10^{-5} megatons). The shock wave reached observers 1.78 minutes after the event, accompanied by a maximum wind velocity of 0.0422 m s^{-1} and sound levels near 25 dB—consistent with witness reports and the observed impact crater. Microscopic and XRF analyses reveal coarse-grained textures with high concentrations of Fe, Si, and Mg. PM-01 contains 23.55% Fe, 20.18% Si, and 12.48% Mg, whereas PM-02 contains 48.09% Fe, 25.06% Si, and 10.21% Mg. Thus, this finding indicates that the specimen's mineralogy is dominated by olivine ((Mg, Fe)$_2$SiO$_4$), confirming that it aligns with the classification of an H7 melt breccia.

Keywords:
Punggur Meteorite; Mineralogic; Chemical; Olivine; Stony; Breccia

Introduction

On January 28, 2021, at 9:53 p.m. local time (UTC + 07.00 hours), residents in southern Sumatra heard loud booms that shook their houses. The Indonesian Tsunami Early Warning System (InaTEWS) recorded the sonic boom. Eyewitnesses report that the bolide was traveling in a W/NW

direction. Several meteorite fragments were found in the Punggur district, Central Lampung, Indonesia. A 2.2 kg stone crashed through the roof and embedded itself in the soil beside a house at 5° 00’ 22.4” S 105° 16’ 11.9” E. That night, a woman found a ~50-gram specimen that reportedly bounced off a nearby roof at 5° 00’ 35.15” S, 105° 13’ 13.90” E. In the following morning, three additional masses were found: a 138-gram mass that crashed through a roof and landed on a bed (4° 59’ 46.6” S 105° 14’ 47.6” E); a ~1700-gram mass in a flooded hole in a rice paddy (4° 59’ 56.2” S 105° 15’ 23.4” E); and, a 2511-gram mass was recovered from a rice paddy (4° 59’ 50.4” S 105° 15’ 13.7” E). The geographical distribution of the five meteorite fragments that fell on January 28, 2021, in Punggur District is shown in **Figure 1**.

Figure 1. Meteorite fall locations map

The Punggur meteorite, which fell in January 2021, has been classified as an H7 melt breccia with a low shock stage and weathering grade W0 (Meteoritical Bulletin, 2021). This classification is relatively uncommon, as H7 breccias represent a rare subset of ordinary chondrites (Rubin et al., 2001; Ruzicka et al., 2005; Bischoff et al., 2006). Meteorite classification relies heavily on mineralogical and petrographic characteristics (Weisberg et al., 2006), yet breccia meteorites that exhibit evidence of melting—such as the Punggur specimen—remain insufficiently described in existing classification schemes. Consequently, further mineralogical investigation of this meteorite is necessary to refine breccia-related classification criteria. Meteoritic breccias provide valuable records of parent body histories, including surface processes, impact events, and thermal metamorphism (Burbine et al., 2002; Keil et al., 1997). These rocks preserve information on accretion, lithologic mixing, excavation, shock heating, partial melting, and subsequent re-accretion. Breccias are generally categorized according to their clast composition and formation processes (Bischoff et al., 2011), including monomict breccias, derived from the fragmentation of a single lithology, and polymict breccias, composed of multiple lithologies embedded within a matrix. Based on its classification as an H7 melt breccia, the Punggur meteorite most closely aligns with monomict breccias, which typically form through localized impact-induced fragmentation and consolidation, followed by thermal sintering during ejecta deposition. Despite its classification, no detailed mineralogical or geochemical study of the Punggur meteorite has been conducted to date. Key questions remain regarding its melt-related textures, elemental composition, and formation conditions within its parent body. Therefore, this study aims to: (1) characterize the mineralogical and chemical composition of the Punggur meteorite using X-ray fluorescence (XRF) and microscopic analysis; (2) evaluate meteoroid atmospheric entry parameters using a web-based impact modeling tool to contextualize the fall event; and (3) compare the Punggur meteorite with other H-group breccias reported in the literature to refine its classification and better understand its formation history.

Methods

Determination of Trajectory and Meteorite Impact on Earth

The determination of orbital elements was carried out with the help of SpiceyPy. SpiceyPy is an open-source Python module that was modified from the previously C-based SPICE toolkit. This module works to solve the equations of orbital elements and also obtain the accurate constants provided by the NASA Navigation and Ancillary Information Facility (NAIF) (Annex et al., 2020). Then, we used a web-based program, developed by Collins et al. (2005) (www.lpl.arizona.edu/impacteffects), to quickly estimate the regional environmental consequences of a comet or asteroid impact on Earth.

Physical and Chemical Properties

The data presented in this study were collected using an Olympus Delta portable X-ray fluorescence (XRF) analyzer. XRF analysis involves using an X-ray source that irradiates the sample, which, in turn, fluoresces due to the atomic excitation of the material. The instrument uses two X-ray beams to avoid spectral-peak superpositions of the sample elements; the first beam measures the elements V, Cr, Fe, Co, Ni, Cu, Zn, W, Hg, As, Se, Pb, Bi, Rb, U, Sr, Y, Zr, Th, Mo, Ag, Cd, Sn, and Sb, while the second measures Mg, Al, Si, P, S, Cl, K, Ca, Ti, and Mn. Then, chemical analysis was performed on the fragment's interior and exterior using the Olympus Delta portable X-ray fluorescence (XRF) analyzer (Hallis et al., 2014; Wittmann et al., 2015; Allegretta et al., 2020). These results were then compared with those of other meteorites.

Additionally, these techniques were used to research the fusion crust from this fragment using optical microscopy and compare it with that of other well-published meteorites. The physical properties measured include magnetism, surface color, weight, volume, density, and porosity (Macke, 2010; Consolmagno et al., 2008). The density is calculated using the volume of water and the mass of the fragments. The simple concept of assuming the amount of water displaced implies that an object immersed in water displaces a volume of water equal to the volume of the object. The rock hardness measurements were made with an index on the Mohs scale. We utilize conventional tools to test the hardness of objects by scratching a clean and fresh surface using the Mohs Hardness Test Kit on each fragment. The fusion crust is present at the fragment's surface and is studied using a stereo microscope.

Results and Discussions

Orbital Reconstruction and Impact Simulation Results

The orbital reconstruction indicates that the pre-entry trajectory of the Punggur meteorite extended from the outer region of the asteroid belt to a point just inside Earth’s orbit (Figure 2). While most meteorites originate from asteroidal bodies, the specific parent-body type of the Punggur meteorite requires further investigation.

The reconstructed orbit suggests that the Punggur meteorite was originally part of a larger planetesimal formed during the early stages of the Solar System. Its trajectory resembles that of Apollo-type Near-Earth Asteroids (NEAs), characterized by high eccentricity and Earth-crossing behavior. In this case, the meteorite's perihelion lies within Earth's orbit, whereas its aphelion extends into the outer asteroid belt. Such orbital geometry places the body at a relatively high likelihood of reaching a Minimum Orbit Intersection Distance (MOID) to intersect Earth's orbital path. Chemical and mineralogical analyses indicate that the meteorite originated from a stony-iron parent body. Both S-type (silicate-rich) and M-type (metal-rich) asteroids are abundant in the inner central belt, consistent with the reconstructed orbit. The semimajor axis of 2.131 au places the parent body near several of Jupiter's mean-motion resonance regions (1:4, 2:7, and 1:3). These resonances are considered dynamically chaotic, enabling bodies to undergo orbital elongation and eventually

evolve into NEA-like trajectories. However, confirming this scenario requires a more detailed study of orbital dynamical evolution.

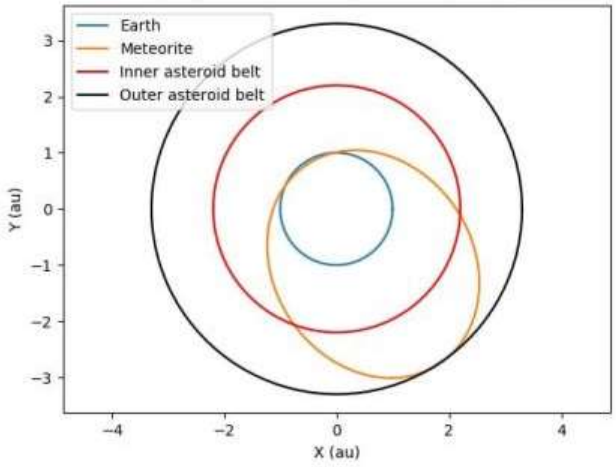

Figure 2. The reconstructed orbital trajectory of the meteorite that fell in Punggur, Lampung, before atmospheric entry

Table 1. Input parameters.

Input Parameters	
Distance from Impact:	2.00 km (1.24 miles)
Projectile diameter:	45.00 cm (17.70 inches)
Projectile Density:	5250 kg m^{-3}
Impact Velocity:	20.80 km s^{-1} (12.90 miles s^{-1})
Impact Angle:	60°
Target Density:	2500 kg m^{-3}
Target Type:	Sedimentary Rock

Eyewitness reports of a bright fireball and a loud explosive sound provided additional constraints for determining the meteor's trajectory. The booming sound is physically explained by the intense pressure gradient generated during hypersonic entry, where the high-pressure region ahead of the meteoroid contrasts sharply with the low-pressure wake behind it, occasionally causing structural disruption as air forces penetrate the body, which can easily blow up some parts. To estimate the environmental effects of the fall, we carried out impact-simulation calculations using physical parameters derived from laboratory measurements. Initial simulations based solely on the properties of individual fragments did not reproduce the observed field evidence, including the absence of a significant crater and the magnitude of the reported sonic boom. To improve the accuracy of the impact modeling, we adjusted the input parameters by treating PM-01 and PM-02 as a single body, rather than assuming they originated from independent meteoroids. Moreover, eyewitness accounts describe a single fireball and a single acoustic event, consistent with the breakup of a unified meteoroid rather than multiple independent falls. A second model, which assumed that the two recovered fragments originated from a single meteoroid that fragmented during atmospheric entry (Table 1), produced results consistent with field measurements and eyewitness descriptions (Table 2). By modeling the object as a single coherent body before fragmentation, the resulting impact parameters more closely match the formed crater morphology, the distribution of recovered

fragments, and the timing and intensity of the acoustic phenomena reported at the fall site. This approach therefore provides a more physically realistic reconstruction of the Punggur meteorite fall event. These findings support the scenario of an airburst-induced breakup before ground impact.

Table 2. Output parameters.

	Result
Energy before atmospheric entry:	5.42×10^{10} Joules = 0.13×10^{-4} MegaTons TNT
The projectile begins to break up at an altitude:	36500 meters = 120000 ft
The projectile bursts into a cloud of fragments at an altitude:	35200 meters = 115000 ft
The residual velocity of the projectile fragments after the burst:	16.2 km s^{-1} = 10.1 miles s^{-1}
The energy of the airburst:	2.12×10^{10} Joules = 0.51×10^{-5} megatons.
The air blast will arrive approximately:	1.78 minutes after impact.
Peak Overpressure:	0.00254 - 0.00508 psi
Max wind velocity:	0.0422 m s^{-1} = 0.0943 mph
Sound Intensity:	25 dB (Easily Heard)

Modeling outputs indicate that, following the airburst event, the projectile fragments retained a substantial residual velocity of approximately 16.2 km s^{-1} (10.1 miles s^{-1}), reflecting the high-energy nature of the meteoroid's atmospheric entry. The airburst released an estimated 2.12×10^{10} J of energy, corresponding to 0.51×10^{-5} megatons, which characterizes the event as a low-yield but dynamically significant atmospheric explosion. The resulting shock wave was predicted to arrive at the observer's location approximately 1.78 minutes after the initial impact. The maximum wind velocity associated with the blast was approximately 0.0422 m s^{-1} (0.0943 mph). Additionally, the event generated an estimated sound intensity of 25 dB, a level classified as easily heard by the human auditory system, and allows for the formation of craters after impact on the Earth's surface. This corresponds to the crater we observed together with the witnesses at the location (See Figure 3), and there was a booming sound, as they described to us.

Figure 3. An impact with one of the meteorite fragments resulted in the formation of a crater.

Physical and Microscopic Properties

For physical and microscopic analyses, the two recovered fragments were designated PM-01 (left side) and PM-02 (right side) (see Figure 4). PM-01 measures 13 × 6.5 × 8 cm, with a volume of 419 mL and a mass of 2200 g, yielding a density of 5.25 ± 0.26 g cm^{-3}. PM-02 measures 25 × 23 × 16 cm, with a volume of 443 mL and a mass of 1820 g, giving a density of 4.06 ± 0.06 g cm^{-3}. The difference in density between the fragments is consistent with their origin as separate parts of a larger meteoroid. Figure 4a shows PM-01, which was found after penetrating the roof of a villager's house upon impact. A small crater, approximately 40 cm deep, was also observed in a rice paddy caused by PM-02. The elongated NW–SE orientation of the crater suggests an incoming azimuth of 312° ± 20° and an impact angle of 59° ± 20°. Baked and compacted clay surrounding the crater indicates high thermal exposure during impact.

Figure 4. Photographs of the Punggur meteorite fragments PM-01(left side) and PM-02 (right side).

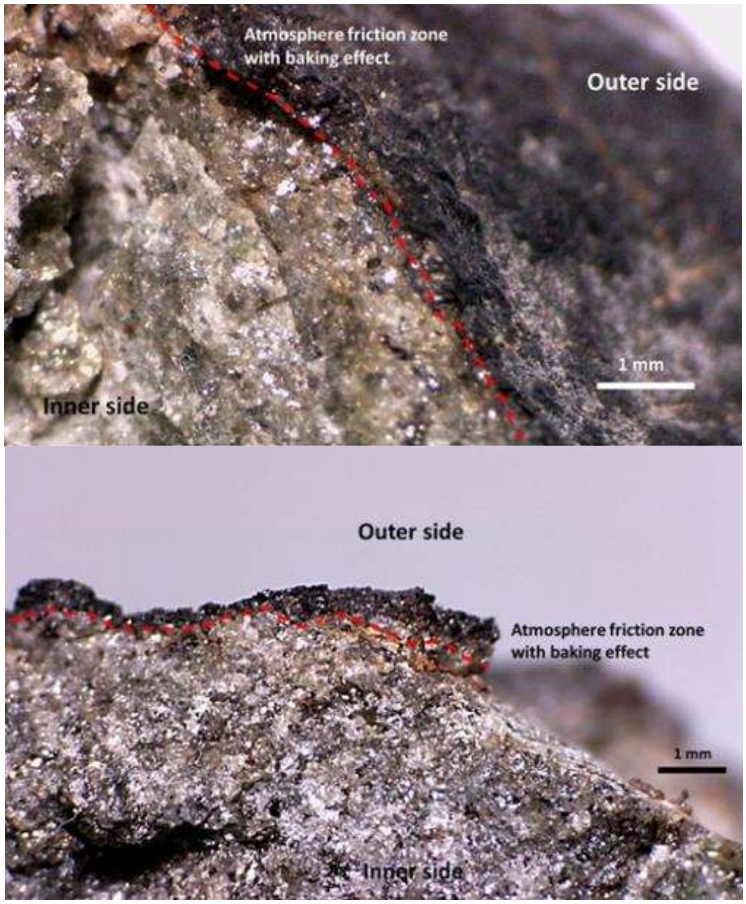

Figure 5. Shown are the fusion crust in Punggur Meteorite fragments PM-01 (*top*) and PM-02 (*bottom*).

Surface hardness measurements further distinguish the two fragments. PM-01 has a dark exterior with a hardness of 4.0–5.0 Mohs, while its interior exhibits an ash-gray color, metallic to dull luster, and a hardness of 5.5–8.0 Mohs. PM-02 has a similarly dark outer surface (with a hardness of 4.0–5.0 Mohs) and a light-gray interior with a hardness of 5.0–7.0 Mohs. Under 40× magnification, both fragments clearly display a fusion crust and associated burn zone (see Figure 5). This thermally altered layer has lower hardness and marks the intense heating generated by atmospheric friction during entry. Localized oxidation is present along surface fractures. The fragments likely remained in the rice field for up to a week before recovery, exposing them to organic-rich water that facilitated aqueous corrosion—dissolved iron ions combined with oxygen to form iron oxides, producing rust on the meteorite surface. Atmospheric corrosion may also contribute, as thin electrolyte films on the metal allow Fe^{2+} ions to oxidize to Fe^{3+}, forming hydrated ferric oxides that act as a partial protective layer. Internally, both fragments exhibit crystalline chondritic textures, containing minerals that range from dark to light and from transparent to opaque, with dominant chondrule sizes of approximately 0.1–0.5 mm.

Geochemical (XRF) Composition

Table 3 Comparative Element Composition of Punggur Meteorite Fragments PM-01 and PM-02

Element	PM-01 (w/w%)		PM-02 (w/w%)	
	Measured	**normalized**	**Measured**	**Normalized**
Fe	23.6	23.5	48.1	48.1
Si	20.2	20.1	25.1	25.1
Mg	12.5	12.4	10.2	10.2
Ca	1.35	1.35	4.20	4.20
Al	2.39	2.38	3.00	3.00
S	1.91	1.90	2.61	2.61
Cr	0.39	0.39	1.05	1.01
Mn	0.28	0.28	0.86	0.86
Cl	0.82	0.82	0.84	0.84
P	0.22	0.22	0.72	0.72
Ni	0.76	0.76	0.52	0.52
Ti	0.05	0.05	0.42	0.42
Zn	0.01	0.01	0.03	0.03
Sn	0.02	0.02	0.02	0.02
Sb	0.02	0.02	0.01	0.01
Pb	0.00	0.00	0.01	0.01
Cd	0.02	0.02	0.00	0.00
Cu	0.01	0.01	0.00	0.00
LE*	35.9	35.8	2.37	2.37
Total	100.4	100.0	100.0	100.0

*LE: Light Elements

Chemical compositions of the meteorite fragments were analyzed using a portable X-ray fluorescence (XRF) spectrometer. Measurements were conducted on both the interior and exterior surfaces. The interior displays a relatively fresh, unweathered condition, with significant elements including Si (27.1–28.3%), Fe (19.8–22.1%), Mg (15.2–17.3%), Al (2.4–2.9%), Ca (1.7–1.9%), and S (0.97–1.0%). Minor elements identified include Mn, Ni, Cr, and P, along with trace quantities of Co, Ti, Sb, Sn, V, Cd, and Zn. The exterior surface exhibits a similar elemental suite but with notable compositional shifts likely resulting from weathering and surface alteration. Major elements include Si (19.0–21.7%), Fe (27.9–29.3%), Mg (10.1–13.3%), Al (4.6–4.9%), and Ca (1.7–1.8%). Minor

elements such as S, Mn, Ni, Cr, and P are present, whereas trace elements Co and V are absent on the exterior, and Cd and Zn appear only in low concentrations. Compared to the interior, the exterior contains higher concentrations of Ni, Fe, Al, Ti, P, and Cd, while sulfur is noticeably reduced. These differences are consistent with oxidation, aqueous alteration, and differential weathering occurring after the meteorite's fall. XRF measurements of the two fragments indicate broadly similar major-element compositions dominated by Fe, Si, and Mg. PM-01 contains 23.55% Fe, 20.18% Si, and 12.48% Mg, whereas PM-02 contains 48.09% Fe, 25.06% Si, and 10.21% Mg. Detailed values are presented in Table 3.

To evaluate the compositional similarity between PM-01 and PM-02, a paired t-test was performed. The Pearson correlation coefficient between corresponding elements is 0.95, with a one-tailed t-critical value of 1.74, t-statistic of -1.35, and p-value of 0.10. These results indicate no statistically significant difference, suggesting that the two fragments are compositionally similar and likely originated from the same parent meteoroid.

Discussion: Classification and Comparison with Other Meteorites.

A comparison with other meteorite groups was performed using a Fe–Si–Mg ternary diagram following the classification scheme of King et al. (2019). The results, summarized in Table 4 and illustrated in Figure 6, plotted alongside the olivine–pyroxene mineral boundary fields, further support the classification of the Punggur meteorite fragments as stony-iron meteoritic. This approach allows the classification of meteorites that have undergone equilibrium silicate melting, particularly those of Type 7 metamorphism (Tait et al., 2014). The Punggur meteorite falls predominantly within the olivine field (see Figure 6). Olivine, a $(Mg, Fe)_2SiO_4$ silicate mineral common in Earth's mantle, is also abundant in many stony meteorites.

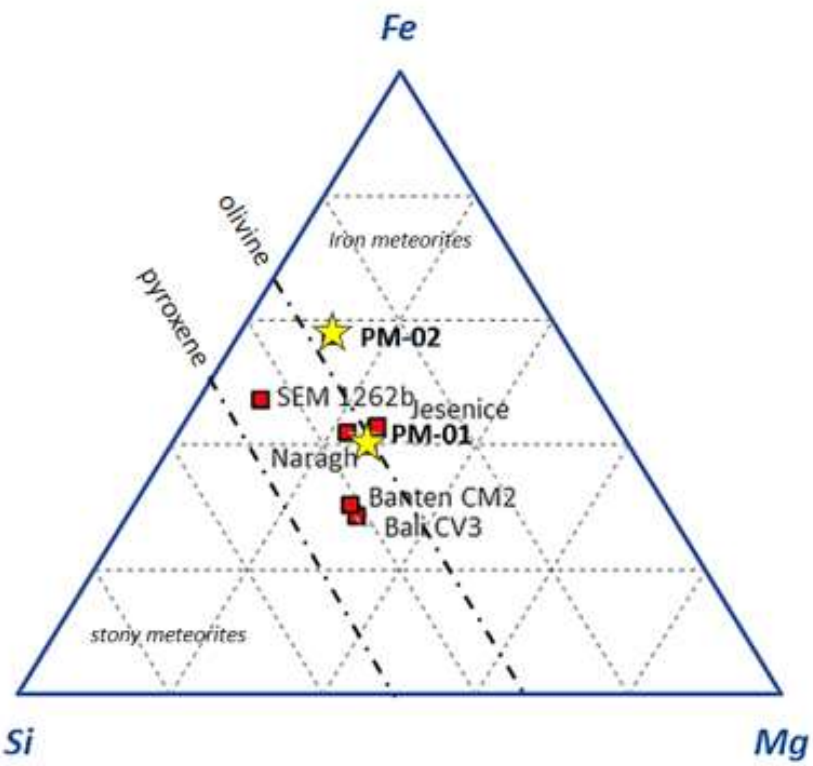

Figure 6: Ternary diagram. Compared the Fe-Mg-Si compositions of the Punggur meteorite (yellow star) and other stony-iron meteorites. A black dotted line represents olivine and pyroxene.

Table 4 Comparative Fe–Si–Mg (w%) Composition of the Punggur Meteorite and Reference Meteorites.

Specimen	Fe (w%)	Si (w%)	Mg (w%)	Reference
PM-01	23.6	20.2	12.5	this study
PM-02	48.1	25.1	10.2	
Bali CV3	23.3	33.8	24.5	[16]
Banten CM2	21.1	28.8	19.8	
SEM 1262b	40.2	37.9	6.8	
Naragh	37.2	31.7	23.8	[17]
Jesenice	23.9	17.5	14.3	[7]

In general, meteorites contain less than 60% SiO_2, whereas many terrestrial rocks exceed this threshold due to the presence of quartz. A rock with SiO_2 content above 60% is therefore unlikely to be a meteorite, as meteorites characteristically lack quartz and other silica-rich minerals. As shown in the four chemical diagrams in Figure 7, focusing on the position of the Punggur sample (yellow box) compared to chondrite H3–H6 and silicate-rich Portales Valley (blue box). SiO_2 vs MgO diagram (upper left panel). The H3–H6 chondrite data form a relatively compact distribution in the range of 34–37 wt% SiO_2 and 21.5–23.5 wt% MgO. The Punggur sample is located in an area with higher SiO_2 (≈ 39 wt%) and lower MgO (≈ 22.7 wt%) than the center of the H3–H6 distribution. This pattern is closer to the composition of silicate-rich Portales Valley, which also has high SiO_2 and more variable MgO. Punggur's position is outside the typical H-chondrite zone, indicating possible silicate enrichment due to melt differentiation. Therefore, Punggur's composition is consistent with shock-melted H-chondrites, rather than typical H3–H6, and potentially closer to H7 melt breccia. The SiO_2 vs Fe(t) diagram (upper right panel) H3–H6 shows a downward trend in Fe(t) with increasing SiO_2. Punggur is again located far to the right, with very high SiO_2 but low Fe(t), outside the H3–H6 field. The position vector of Punggur is similar to the direction of deviation of the Portales Valley sample. Therefore, the lower Fe(t) value than H-chondrite indicates a more Mg-rich Olivine content, suggesting the presence of high metamorphism. The MgO vs Fe(t) diagram (lower left panel) H3–H6 shows a correlational pattern, where FeO decreases as MgO increases. Punggur is located at high MgO (≈ 23 wt%) but high Fe(t)—outside the H-chondrite distribution. This position is consistent with silicate-rich Portales Valley samples, which also exhibit Fe/Mg shifts due to melt–silicate fractionation processes. Therefore, the MgO–Fe(t) relationship indicates a change in the Fe/Mg ratio during melting and recrystallization, consistent with H-melt breccia rather than typical H5–H6. The Total Fe(t) vs. Total Major Silicate diagram (bottom right panel) shows that H3–H6 have a controlled trend reflecting equilibrated silicates. Punggur is located far to the right (high total silicate), and Fe(t) is relatively high, shifting its position outside the primary distribution. The direction of the deviation is consistent with the silicate-rich trend of Portales Valley. Thus, this position reinforces that Punggur has a higher silicate content than H-chondrite, indicating a melt-silicate component separate from the metal, which is similar to the H7 melt breccia.

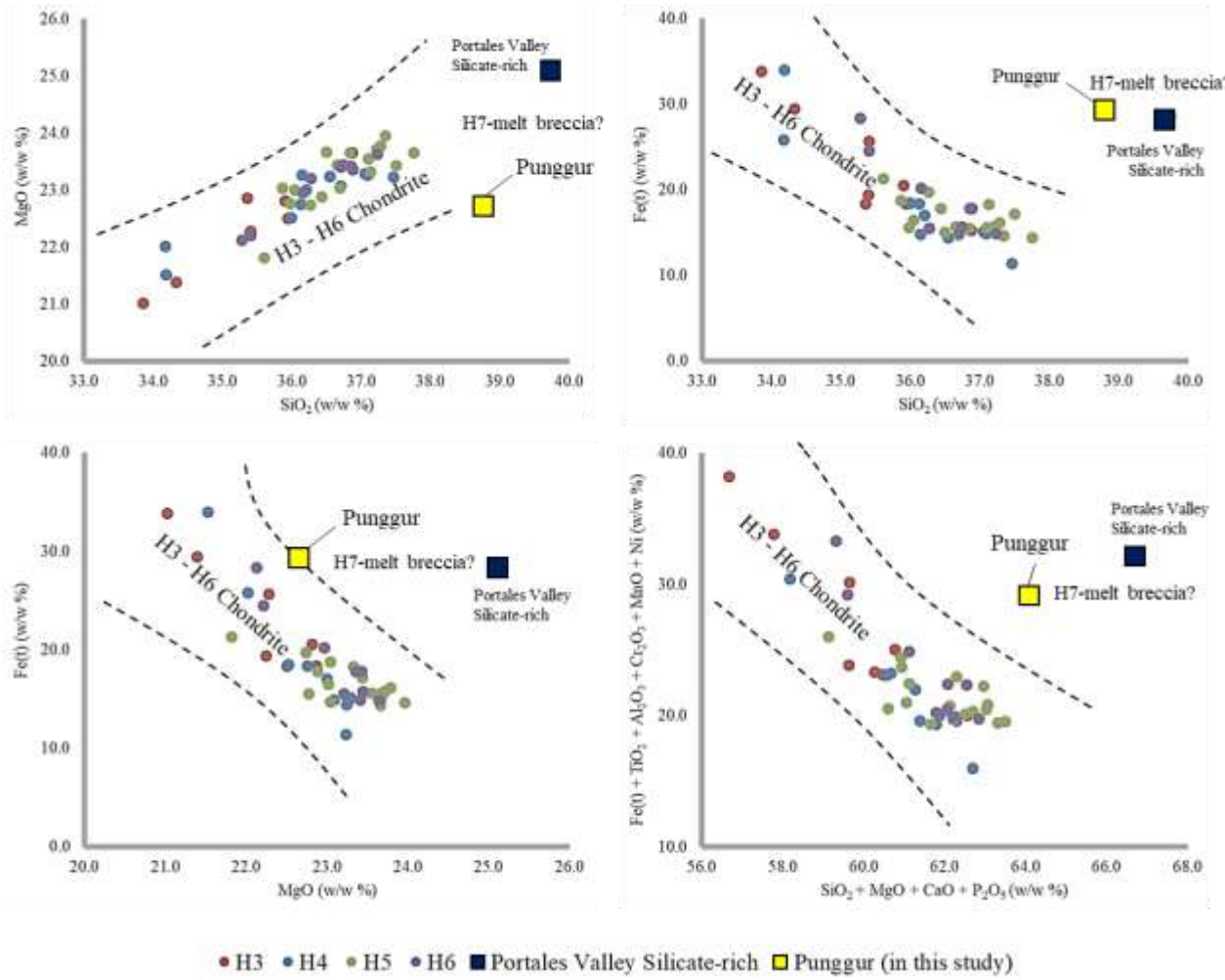

Figure 7. A plot diagram of the Punggur Meteorite's chemical composition with other H-chondrite meteorites

A comparison of additional components is provided in Table 5. Variations in Fe(t) and MgO contents are beneficial for distinguishing terrestrial rocks from meteorites. Based on these geochemical signatures, the specimen recovered from Punggur Village is confirmed to be a meteorite and shows substantial compositional similarity to the Portales Valley meteorite.

Table 5. Comparative Chemical Composition (w%) of the Punggur Meteorite and Other H-Chondrites

Meteorite	Class	SiO_2	TiO_2	Al_2O_3	Cr_2O_3	Fe(t)	MnO	MgO	CaO	Ni	*A*	*b*	Ref.
Punggur	**H7-Melt**	**38.76**	**0.06**	**3.70**	**0.46**	**29.15**	**0.5**	**22.6**	**2.51**	**0.48**	**64.07**	**34.35**	**this study**
ALHA77299	H3	35.94	0.11	2.27	0.41	18.38	0.30	22.50	1.81	1.67	60.47	23.14	(Taid et al., 2014)
Clovis	H3	35.40	0.10	2.06	0.46	25.67	0.31	22.28	1.64	1.56	59.65	30.16	
Dhajala	H3	36.87	0.12	2.14	0.56	15.31	0.32	23.66	1.74	1.58	62.56	20.03	
Sharps	H3	35.39	0.12	1.90	0.45	19.41	0.30	22.24	1.71	1.70	59.63	23.88	
Study Butte	H3	34.33	0.13	2.06	0.50	29.48	0.28	21.39	1.81	1.38	57.77	33.83	
Willaroy	H3	33.85	0.13	2.13	0.48	33.83	0.27	21.02	1.61	1.37	56.67	38.21	
Conquista	H4	35.99	0.11	2.07	0.47	18.48	0.31	22.52	1.73	1.64	60.54	23.08	

Meteorite	Class	SiO_2	TiO_2	Al_2O_3	Cr_2O_3	Fe(t)	MnO	MgO	CaO	Ni	*A*	*b*	Ref.
Punggur	**H7-Melt**	**38.76**	**0.06**	**3.70**	**0.46**	**29.15**	**0.5**	**22.6**	**2.51**	**0.48**	**64.07**	**34.35**	**this study**
Farmville	H4	37.05	0.11	2.09	0.50	15.10	0.33	23.29	1.66	1.82	62.26	19.95	
Faucett	H4	36.12	0.11	2.21	0.53	18.38	0.29	22.75	1.54	1.70	60.66	23.22	
Forest Vale	H4	37.46	0.13	1.98	0.46	11.38	0.31	23.23	1.69	1.76	62.69	16.02	
Kabo	H4	36.54	0.12	2.15	0.53	14.42	0.33	23.24	1.72	1.80	61.78	19.35	
Kiffa	H4	36.14	0.12	2.14	0.52	14.77	0.31	23.26	1.77	1.77	61.39	19.63	
Marilia	H4	37.09	0.11	2.06	0.49	14.92	0.32	23.26	1.66	1.71	62.28	19.61	
Schenectady	H4	36.20	0.12	2.25	0.55	17.06	0.32	23.00	1.77	1.72	61.26	22.02	
ALHA77294	H5	37.75	0.14	2.31	0.57	14.38	0.33	23.66	1.83	1.84	63.49	19.57	
Allegan	H5	36.69	0.10	1.95	0.54	14.70	0.30	23.04	1.65	1.76	61.65	19.35	
Ashmore	H5	36.43	0.11	2.00	0.55	17.82	0.29	22.88	1.60	1.70	61.11	22.47	
Bonita Springe	H5	36.04	0.11	1.96	0.47	16.49	0.33	23.01	1.62	1.64	61.05	21.00	
Burdett	H5	35.60	0.12	2.07	0.53	21.34	0.30	21.82	1.48	1.68	59.13	26.04	
Chela	H5	37.34	0.12	2.23	0.48	14.63	0.30	23.96	1.76	1.73	63.31	19.49	
Ehole	H5	36.84	0.14	2.02	0.49	15.55	0.29	23.66	1.76	1.64	62.51	20.13	
Ipiranga	H5	37.10	0.12	2.17	0.52	15.58	0.27	23.55	1.77	1.68	62.68	20.34	
Lost city	H5	36.49	0.12	2.08	0.53	15.04	0.29	23.67	1.72	1.65	62.21	19.71	
Macau	H5	36.26	0.11	2.02	0.52	19.76	0.32	22.74	1.65	1.68	60.91	24.41	
Oro Grande	H5	34.18	0.14	1.83	0.55	34.00	0.31	21.52	1.72	1.46	57.67	38.29	
Pribram	H5	37.22	0.11	2.10	0.50	15.81	0.30	23.72	1.79	1.68	63.02	20.50	
Pulsora	H5	35.97	0.12	2.26	0.52	15.57	0.29	22.77	1.59	1.78	60.59	20.54	
Sitathali	H5	36.65	0.14	2.37	0.43	15.72	0.31	23.45	1.71	1.79	62.11	20.76	
Uberaba	H5	37.50	0.12	2.30	0.55	17.22	0.32	23.43	1.78	1.73	62.96	22.24	
Ucera	H5	37.28	0.11	2.10	0.52	16.18	0.31	23.78	1.74	1.67	63.06	20.89	
Abbott	H6	36.15	0.12	2.25	0.45	20.23	0.31	22.96	1.77	1.52	61.11	24.88	
ALHA76008	H6	35.40	0.10	2.14	0.45	24.53	0.30	22.21	1.68	1.71	59.59	29.23	
ALHA77271	H6	36.88	0.11	1.97	0.50	17.85	0.28	23.36	1.60	1.69	62.06	22.40	
Andura	H6	36.85	0.16	1.85	0.53	17.80	0.39	23.42	1.97	1.62	62.53	22.35	
Butsura	H6	36.27	0.12	1.98	0.56	15.54	0.31	23.21	2.00	1.75	61.79	20.26	
Canon City	H6	36.70	0.14	2.10	0.54	14.93	0.34	23.41	1.80	1.82	62.21	19.87	
Chiang Khan	H6	37.23	0.13	2.30	0.50	14.85	0.32	23.64	1.73	1.66	62.84	19.76	
Guarena	H6	36.74	0.12	2.04	0.55	15.72	0.32	23.44	1.60	1.74	62.05	20.49	
Mills	H6	35.27	0.12	2.45	0.47	28.38	0.28	22.13	1.68	1.63	59.31	33.33	
Portales Valley Si-rich	H6-7	39.77	0.13	2.20	0.43	28.50	0.33	25.13	1.61	0.15	66.66	31.74	(Ruzicka et al., 2005)

* note: $a = SiO_2 + MgO + CaO + P_2O_5$ $b = Fe(t) + Ni + TiO_2 + Al_2O_3 + Cr_2O_5 + MnO$

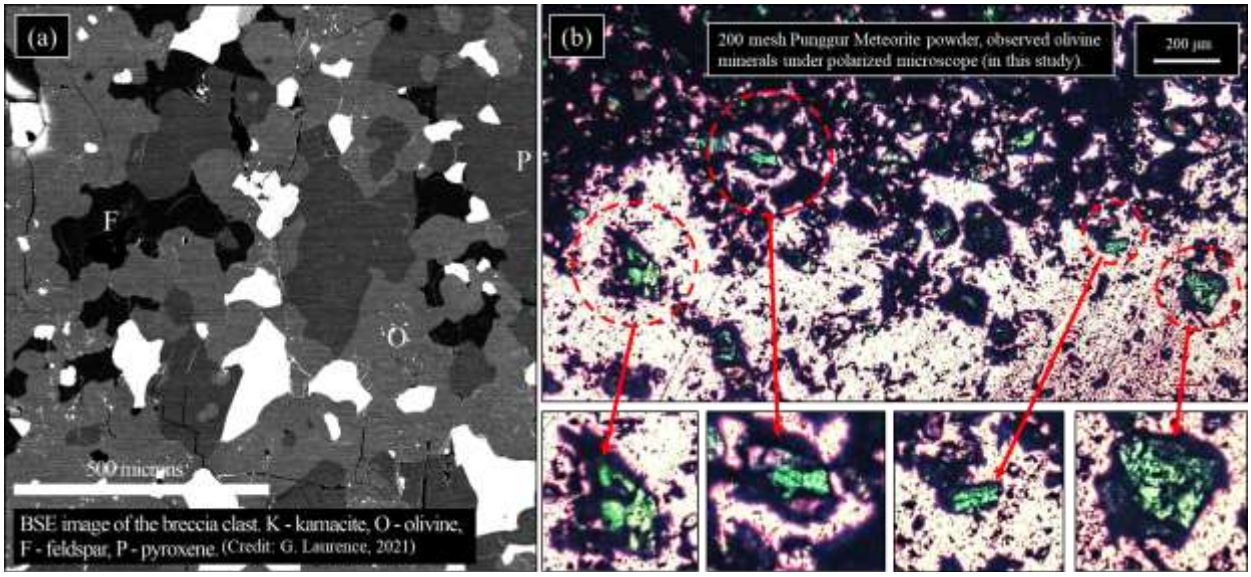

Figure 8 The micron-size image of the Punggur meteorite, (a) the backscattered electron image (BSE) of the polished surface [18], and (b) 200-mesh powder observed in the polarized microscope (this study)

Microscopic analysis (Figure 8a) reveals an interconnected plagioclase network accompanied by abundant olivine, kamacite, and pyroxene. Corresponds to the measured Fe(t) (29.15%) and Ni (0.48%) contents. Chemical parameters may also aid in classification: orthopyroxene with CaO > 1.0% is characteristic of Type 7 metamorphism [20], which is consistent with the CaO concentrations measured in the orthopyroxene cores of the Punggur sample, reaching up to 2.51% (Table 5). Furthermore, A 200-mesh powder sample was examined using a polarized light microscope to identify its mineralogical components (see Figure 8b). Under cross-polarized illumination, the specimen displays distinct greenish interference colors characteristic of olivine. This observation confirms the presence of olivine as a dominant silicate phase in the powdered material. The green coloration arises from olivine's birefringence and optical properties, which commonly produce first-order interference hues in fine-grained or powdered samples. Identifying olivine in the 200-mesh fraction is consistent with the mineralogy expected from ordinary chondrite meteorites, particularly those of the H-group, which typically contain abundant olivine as a primary mafic silicate. These results support the broader petrographic and geochemical evidence obtained in this study, strengthening the interpretation that the sample is olivine-rich and consistent with the classification proposed for the Punggur meteorite. Overall, the mineralogical, chemical, and textural characteristics support the classification of the Punggur meteorite as H7 melt breccia, consistent with its listing in the Meteoritical Bulletin (2021).

Conclusions

This study provides the first systematic scientific characterization of the Punggur meteorite fragments recovered from the January 28, 2021, fall in Lampung, Indonesia. Physical measurements, Orbital recontructions, and geochemical analyses collectively confirm the extraterrestrial origin of the specimens. The two analyzed fragments, PM-01 and PM-02, exhibit density values, hardness ranges, and fusion-crust features typical of chondrites. Microscopic observations reveal well-defined heat-affected zones, metallic oxidation features, and coarse-grained textures composed predominantly of olivine, pyroxene, and kamacite. X-ray fluorescence (XRF) analysis shows that both fragments exhibit major elemental compositions dominated by Fe, Si, and Mg, with a high degree of correlation ($r = 0.95$), indicating that PM-01 and PM-02 originated from the same parent meteoritic

body. When compared with known meteorites, particularly the Portales Valley sample, the Punggur meteorite displays comparable SiO_2, Fe(t), and MgO concentrations. The Fe–Si–Mg ternary relationships, combined with the mineralogical indicators—including CaO contents in orthopyroxene and the dominance of olivine—support classification within the H-chondrite group.

These integrated results are consistent with the official classification reported in the Meteoritical Bulletin (2021), which identifies the Punggur fall as an H7 melt breccia formed through high-temperature metamorphic and impact processes. This study not only validates that classification but also provides new physical, chemical, and petrographic data that fill a previous gap in documentation for this meteorite fall event. The findings contribute to a more comprehensive understanding of the Punggur meteorite's formation history, its structural characteristics, and its significance within the broader context of ordinary chondrite evolution.

Several aspects of the Punggur meteorite warrant further investigation. High-precision mineral chemistry (e.g., electron microprobe analyses of olivine Fa, pyroxene Fs, and Co–Ni metal phases) is necessary to refine its exact position within the H-chondrite Type 7 classification. Detailed shock-stage determination using Raman spectroscopy and EBSD would improve constraints on its thermal history and the extent of melt generation. These future research directions will enhance the understanding of the Punggur meteorite's formation, its parent body processes, and its significance within the broader context of high-grade metamorphosed chondritic breccias.

References

Adib, D., & Liou, J. G. (1979). The Naragh Meteorite: A new olivine-bronzite chondrite fall. Meteoritics, 14(3), 257-272. https://doi.org/10.1111/j.1945-5100.1979.tb00502.x

Allegretta, I., Marangoni, B., Manzari, P., Porfido, C., Terzano, R., De Pascale, O., & Senesi, G. S. (2020). Macro-classification of meteorites by portable energy dispersive X-ray fluorescence spectroscopy (pED-XRF), principal component analysis (PCA) and machine learning algorithms. Talanta, 212, 120785. https://doi.org/10.1016/j.talanta.2020.120785

Annex, A. M., Pearson, B., Seignovert, B., Carcich, B. T., Eichhorn, H., Mapel, J. A., ... & Murakami, S. Y. (2020). SpiceyPy: A Pythonic wrapper for the SPICE toolkit. Journal of Open Source Software, 5(46), 2050. https://doi.org/10.21105/joss.02050

Bischoff, A., Jersek, M., Grau, T., Mirtic, B., Ott, U., Kučera, J., Horstmann, M., Laubenstein, M., Herrmann, S., Řanda, Z., & Weber, M. (2011). Jesenice—A new meteorite fall from Slovenia. Meteoritics & Planetary Science, 46(6), 793-804. https://doi.org/10.1111/j.1945-5100.2011.01191.x

Bischoff, A., Scott, E. R., Metzler, K., & Goodrich, C. A. (2006). Nature and origins of meteoritic breccias. In D. S. Lauretta & H. Y. McSween Jr. (Eds.), Meteorites and the early solar system II (pp. 679-712). University of Arizona Press. https://www.lpi.usra.edu/books/MESSII/9013.pdf

Burbine, T. H., McCoy, T. J., Meibom, A., Gladman, B., & Keil, K. (2002). Meteoritic parent bodies: Their number and identification. In W. F. Bottke Jr., A. Cellino, P. Paolicchi, & R. P. Binzel (Eds.), Asteroids III (pp. 653-667). University of Arizona Press. https://doi.org/10.1016/S0016-7037(00)00516-0

Collins, G. S., Melosh, H. J., & Marcus, R. A. (2005). Earth impact effects program: A web-based computer program for calculating the regional environmental consequences of a meteoroid impact on Earth. Meteoritics & Planetary Science, 40(6), 817-840. https://doi.org/10.1111/j.1945-5100.2005.tb00157.x

Consolmagno, G. J., Britt, D. T., & Macke, R. J. (2008). The significance of meteorite density and porosity. Geochemistry, 68(1), 1-29. https://doi.org/10.1016/j.chemer.2008.01.003

Dodd, R. T., Grover, J. E., & Brown, G. E. (1975). Pyroxenes in the Shaw (L-7) chondrite. Geochimica et Cosmochimica Acta, 39(12), 1585-1594. https://doi.org/10.1016/0016-7037(75)90081-2

Garvie, L. (2021, July). Punggur (H7-melt breccia) [Photograph]. The Meteoritical Society. https://www.lpi.usra.edu/meteor/get_original_photo.php?recno=5676235

Hallis, L. J., Ishii, H. A., Bradley, J. P., & Taylor, G. J. (2014). Transmission electron microscope analyses of alteration phases in Martian meteorite MIL 090032. Geochimica et Cosmochimica Acta, 134, 275-288. https://doi.org/10.1016/j.gca.2014.02.007

Jarosewich, E. (1990). Chemical analyses of meteorites: A compilation of stony and iron meteorite analyses. Meteoritics, 25(4), 323-337. https://doi.org/10.1111/j.1945-5100.1990.tb00717.x

Keil, K., Stoeffler, D., Love, S. G., & Scott, E. R. D. (1997). Constraints on the role of impact heating and melting in asteroids. Meteoritics & Planetary Science, 32(3), 349-363. https://doi.org/10.1111/j.1945-5100.1997.tb01278.x

King, A. J., Bates, H. C., Krietsch, D., Busemann, H., Clay, P. L., Schofield, P. F., & Russell, S. S. (2019). The Yamato-type (CY) carbonaceous chondrite group: Analogues for the surface of asteroid Ryugu? Geochemistry, 79(4), 125531. https://doi.org/10.1016/j.chemer.2019.08.003

Macke, R. J. (2010). Survey of meteorite physical properties: Density, porosity and magnetic susceptibility [Doctoral dissertation, University of Central Florida]. STARS. https://stars.library.ucf.edu/etd/1638

Rubin, A. E., Ulff-Møller, F., Wasson, J. T., & Carlson, W. D. (2001). The Portales Valley meteorite breccia: Evidence for impact-induced melting and metamorphism of an ordinary chondrite. Geochimica et Cosmochimica Acta, 65(2), 323-342. https://doi.org/10.1016/S0016-7037(00)00516-0

Ruzicka, A., Killgore, M., Mittlefehldt, D. W., & Fries, M. D. (2005). Portales Valley: Petrology of a metallic-melt meteorite breccia. Meteoritics & Planetary Science, 40(2), 261-295. https://doi.org/10.1111/j.1945-5100.2005.tb00380.x

Tait, A. W., Tomkins, A. G., Godel, B. M., Wilson, S. A., & Hasalova, P. (2014). Investigation of the H7 ordinary chondrite, Watson 012: Implications for recognition and classification of Type 7 meteorites. Geochimica et Cosmochimica Acta, 134, 175-196. https://doi.org/10.1016/j.gca.2014.02.039

Weisberg, M. K., McCoy, T. J., & Krot, A. N. (2006). Systematics and evaluation of meteorite classification. In D. S. Lauretta & H. Y. McSween Jr. (Eds.), Meteorites and the early solar system II (pp. 19-52). University of Arizona Press.

Wittmann, A., Korotev, R. L., Jolliff, B. L., Irving, A. J., Moser, D. E., Barker, I., & Rumble III, D. (2015). Petrography and composition of Martian regolith breccia meteorite Northwest Africa 7475. Meteoritics & Planetary Science, 50(2), 326-352. https://doi.org/10.1111/maps.12425